Optimization of Interior Art Design Space Engineering Technology Based on Digital Twin Modeling

Jingjing Tao
Department of Art and Design, City University of Wuhan, Wuhan 430083, Hubei, China
Corresponding author: Jingjing Tao (e-mail: ami103030@163.com)

ABSTRACT Accurate perception and dynamic optimization of intelligent indoor environments are increasingly important for digital engineering systems integrating sensing, communication, and physical space management. To overcome the separation between aesthetic design and engineering performance in conventional interior design, this study proposes a multiobjective collaborative optimization framework based on digital twin modeling. A dynamic Building Information Modeling (BIM) twin is established by integrating Internet of Things (IoT) sensing data, while convolutional neural networks are employed to extract visual feature representations of interior scenes. Computational Fluid Dynamics and Finite Element Analysis are incorporated to evaluate thermal comfort and structural safety, and an improved NSGA-III algorithm performs global optimization of aesthetic quality, energy efficiency, and engineering constraints. Experimental results demonstrate that the proposed framework achieves a hypervolume value of 0.8978 after 500 iterations, with aesthetic scores reaching 8.74 and compliance rates of 96.4% for thermal comfort, 98.2% for structural safety, and 95.8% for energy consumption. By coupling real-time sensing information with digital twin feedback and multi-physics simulation, the proposed approach establishes a closed-loop optimization paradigm for intelligent indoor environments, providing a scalable methodology for electromagnetic sensing-assisted spatial perception, networked digital twins, and engineering optimization in smart built environments.

INDEX TERMS digital twin modeling; electromagnetic sensing; intelligent indoor environment; multi-objective optimization; networked spatial perception

I. INTRODUCTION

As its name indicates, interior space design contains both art and engineering. Such inherent unity should be the pursuing direction of design, but the specialized refinement of aesthetics and the cognitive stabilization mechanism driven by human experience produce a linear separation in practice. In practice, current industry usually presents a linear separation between aesthetic value and engineering, leading to structural conflicts and performance quality drop in construction [1-2], that is, construction often involves repeated demolition and material waste. Digital twin modeling technology, which constructs a high-fidelity virtual mirror of a physical object, offers an opportunity to integrate all design knowledge [3-4]. A collaborative design method based on both aesthetic effect and engineering indicator becomes a significant scientific issue. A data-driven design system based on spatial indices meets the digitalization trend of the construction industry. As decision made at design stage could greatly influence the whole life-cycle cost, optimizing the physical construction process through virtual iteration can possess obvious economic benefit and social significance. The research community's attention transfers from single-discipline simulation to multidisciplinary integration. Quantitative expression of aesthetic value is unclear.

Aesthetic elements in interior design including compositional rhythm and color harmony are subjectively perceived from visual effects [5-6]. Existing studies find it difficult to directly convert them into mathematical models associated with physical parameters. Artistic evaluation is divorced from the context of technical optimization [7]. The dynamic response of engineering indicators has multidimensional coupling characteristics [8]. Engineering temperature and humid environment, organization of airflow, and structural stress of interior are not independent. Indicators of interior performance are simultaneously influenced by the realtime interaction of spatial form, interface material, and equipment system [9-10]. Engineering simulation methods based on static calculation or independent operation condition are difficult to accurately predict the engineering dynamic behavior under multi-physics coupling [11]. There is a lack of crosslink between art and engineering. Most of the current parametric design tools are focused on creating geometric forms. BIM maintains a document-centric static database that records design information at discrete moments [12]. This static representation captures neither the continuous variation of environmental states nor the dynamic response of physical parameters. The proposed digital twin framework builds upon the geometric and material foundation of BIM while embedding a time-varying attribute mapping mechanism. IoT data streams continuously update BIM primitives through dynamic mapping functions, transforming a static record into a living virtual mirror that synchronizes with physical space states. This transition from static baseline to dynamic twin enables automated multi-objective optimization across design variables. The trade-off between artistic effects and engineering indicators relies on manual trial and error. Neither efficiency nor optimality of the solution can be guaranteed. The multiphysics simulation data interface lacks an effective mechanism to support it. The academic community has explored multiple paths. In the field of art quantification, some studies have introduced computer vision methods and used CNNs to extract features of the style and composition of design images [13-14]. The output is mostly limited to classification or clustering results [15], and has failed to establish a direct mapping relationship with physical index parameters [16]. Although these methods can identify image style and composition, they stop at the level of visual analysis and fail to embed the extracted features as computable parameters into the model-driven design process. In the engineering simulation level, CFD and FEA have been maturely applied to independent verification of indoor environment and structural safety [17-18]. The simulation process is time-consuming, and the interpretation of results requires professional knowledge. It is difficult to be adopted in real time by the design front end to drive morphological correction. In terms of collaborative optimization, parametric design platforms based on genetic algorithms have been tried to solve optimization problems of single index targets such as lighting or energy consumption [19-20]. Research on incorporating aesthetic effects as equally weighted targets into the multi-objective optimization framework has not yet formed a mature technical path. Existing algorithms often get stuck in local optima when facing the non-continuous and non-convex fitness function of aesthetic index. There is a lack of effective mechanisms for processing multi-physics simulation data interfaces. Current methodologies have not yet established an end-to-end integration of art quantification models, high-precision engineering simulations, and global optimization algorithms. This prevents the creation of a closed loop within a digital twin environment that allows for the synchronous iteration of artistic concepts and engineering metrics. To address the challenge of balancing aesthetic effect and engineering performance indicators in the design phase, this study introduces a multi-objective optimization method based on digital twin modeling. A dynamic BIM twin integrating real-time environmental data from the Internet of Things (IoT) is constructed. A CNN pre-trained with scene images is used to map the visual composition of the design scheme into aesthetic parameters. CFD and FEA solvers are integrated to calculate thermal comfort prediction PMV and stress fields at key structural components, respectively. Aesthetic parameters, PMV values, structural safety factor, and energy consumption per unit area are constructed as multi-dimensional objective functions. A Pareto front search driven by an improved NSGA-III is used to obtain a solution set that balances artistic effect and engineering performance indicators. Optimized parameters are fed back to the digital twin model for virtual verification. The study theoretically achieves a quantitative fusion of aesthetic elements and engineering rational indicators. Technically, a closed-loop iterative architecture for design simulation optimization is constructed, providing a systematic solution to overcome the linear limitations of traditional interior design processes. The entire optimization workflow executes in a design phase virtual mirror without requiring physical space interventions during or after construction.

II. A DIGITAL TWIN-DRIVEN COLLABORATIVE OPTIMIZATION FRAMEWORK

A. DIGITAL RECONSTRUCTION AND DYNAMIC DATA MAPPING OF SPACE PHYSICAL INFORMATION

The static basic model of indoor space geometry, topology, and material properties relies on the fusion mechanism of 3D laser scanning technology and BIM. The 3D laser scanner acquires high-density point cloud data of the indoor space, and the point cloud registration is completed by the iterative nearest point algorithm to eliminate acquisition errors and unify the coordinate system [21-22]. The minimized error function in the registration process is defined as the mathematical expression of the accuracy of spatial geometric reconstruction.

$$E_{\text{reg}} = \sum_{i=1}^{N} \left\| R \cdot p_i + \delta - q_i \right\|^2 \tag{1}$$

E_{reg} represents the registration error value; N is the number of point pairs in the point cloud set; p_i represents the i-th coordinate point in the source point cloud; q_i represents the corresponding coordinate point in the target BIM model; R is the rotation matrix; δ is the translation vector. After geometric reconstruction, the material property information is matched with the parameters of the BIM family library based on the scanning reflection intensity to construct a static digital base integrating physical properties. The IoT sensor network is responsible for collecting real-time environmental data, and the data acquisition protocol adopts the MQTT (Message Queuing Telemetry Transport) protocol to achieve high-concurrency transmission under low bandwidth [23-24]. Sensor nodes are deployed at key spatial locations to continuously monitor temperature, humidity, and illuminance parameters and generate state vectors with timestamps.

$$S_t = [T_t, H_t, L_t, \tau']^T \tag{2}$$

S_t represents the environmental state vector at time t; T_t is the temperature reading; H_t is the humidity reading; L_t is the illuminance reading; τ' is the timestamp of data acquisition. The static BIM model and dynamic IoT data stream are bound together by a unique identifier, establishing a mapping relationship between physical entities and virtual images [25-26]. The digital twin integrates time-varying attribute mapping capabilities, updating sensor data to the corresponding primitive attributes of the BIM model in real time through a data interface [27-28]. The state update of the virtual image follows a dynamic mapping function, which describes the driving logic of physical parameter changes on the virtual model attributes.

$$A_{\text{virt}}(t) = A_{\text{static}} + \eta \cdot (S_t - S_{\text{base}}) \tag{3}$$

$A_{\text{virt}}(t)$ represents the virtual model attribute value at time t; A_{static} is the static baseline attribute value; η is the data mapping coefficient; S_{base} is the environmental baseline state vector. The mapping mechanism maintains the synchronization between the geometric information in the virtual space and the environmental state in the physical space, constructing a high-fidelity dynamic twin. The data flow follows a layered architecture: physical space data is transmitted to the processing layer via a sensor network, processed, and written into the BIM database, and finally presented in the virtual mirror layer. The entire reconstruction and mapping process does not involve subjective intervention and is entirely data-driven to complete the model update.

Figure 1 shows the hierarchical data flow and mapping relationships between physical space, sensor networks, BIM and virtual mirrors. The main body includes a physical entity layer, a data acquisition layer, a processing and mapping layer, and a virtual mirror layer. 3D laser-scanned point clouds based on iterative nearest-point algorithm are written and then uploaded into BIM static model; environmental state vectors are sent from IoT sensor networks to the cloud through MQTT protocol; unique identifier binding and dynamic mapping function calculation in the processing layer are finished; attribute value in virtual mirror layer is updated, and static geometric information with dynamic environmental state is synchronized through above procedure.

B. QUANTIFICATION AND PARAMETRIC EXPRESSION OF VISUAL FEATURES OF DESIGN AESTHETIC ELEMENTS

The panoramic rendered view generated by the digital twin model constitutes the input tensor of the CNN. The network architecture loads weight parameters pre-trained on a scene image dataset. The CNN employs a ResNet50 backbone pre-trained on the ImageNet dataset. The network consists of five residual blocks containing convolutional layers with 3 by 3 kernels and filter counts increasing from 64 to 2048. Global average pooling compresses each feature map into a 2048 dimensional vector. Two fully connected layers with 512 and 128 neurons transform this vector into a 16 dimensional aesthetic descriptor. Each dimension of the descriptor corresponds to a quantified aesthetic attribute of compositional balance, rhythmic progression, color harmony, and focal emphasis. The network is trained on a curated dataset of 10000 interior scene renderings. Each rendering is annotated with normalized aesthetic scores derived from pairwise comparisons using a Bradley Terry model. The Adam optimizer minimizes the mean squared error loss between predicted and target vectors with a learning rate of 0.0001 and a batch size of 32 over 100 epochs. Early stopping based on validation loss prevents overfitting. The mathematical expression of a convolutional layer is defined as a discrete convolution operation between the input data and kernel weights, and the output feature map Fis determined by the following formula:

$$F_{i,j}^k = \sum_{m=0}^{K_h-1} \sum_{n=0}^{K_w-1} I_{i+m,j+n} \cdot W_{m,n}^k + \theta_k \tag{4}$$

I represents the input image tensor; W represents the convolution kernel weight matrix; θ is the bias scalar; i, j refer to the spatial coordinate indices of the output feature map; m, n are the convolution kernel offsets; k is the filter index; K_h, K_w represent the height and width of the convolution kernel, respectively. After the feature map is processed by the activation function, it enters the pooling layer. The spatial dimension is reduced through region aggregation. The calculation process of the main feature response value H is as follows:

$$H_k = \frac{1}{|\Omega|} \sum_{(u,v)\in\Omega} F_{u,v}^k \tag{5}$$

Ω represents the set of coordinates in the feature map space; $|\Omega|$ is the window size; u, v represent the local coordinates within the window; and $F_{u,v}^k$ is the feature activation values at the corresponding locations. The fully connected layer maps the pooled feature vectors to the aesthetic evaluation space, generating the final design quality description vector V_{out}. The mapping relationship is given by the following equation:

$$V_{\text{out}} = M_{\text{dense}} \cdot H_{\text{concat}} + b_{\text{dense}} \tag{6}$$

M_{dense} is the weight matrix of the fully connected layer; H_{concat} represents the concatenated high-dimensional feature vector; b_{dense} is the bias vector of the fully connected layer.

Figure 2 shows the activation intensity distribution of the convolutional layers, covering various functional space types. The living room scene is shown in Figure 2(a), with high activation areas distributed along the sofa outline and the boundary of the floor covering. High-intensity response values are triggered by the window light incidence

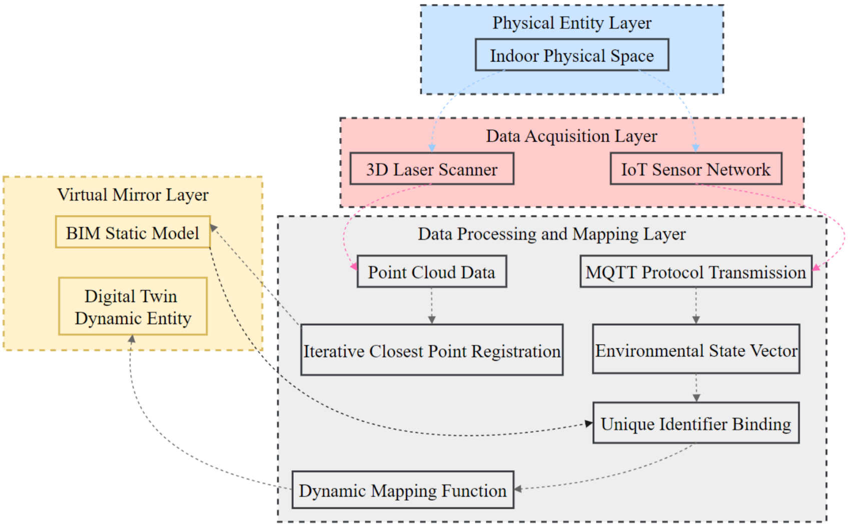

FIGURE 1. Digital Twin Data Fusion Architecture

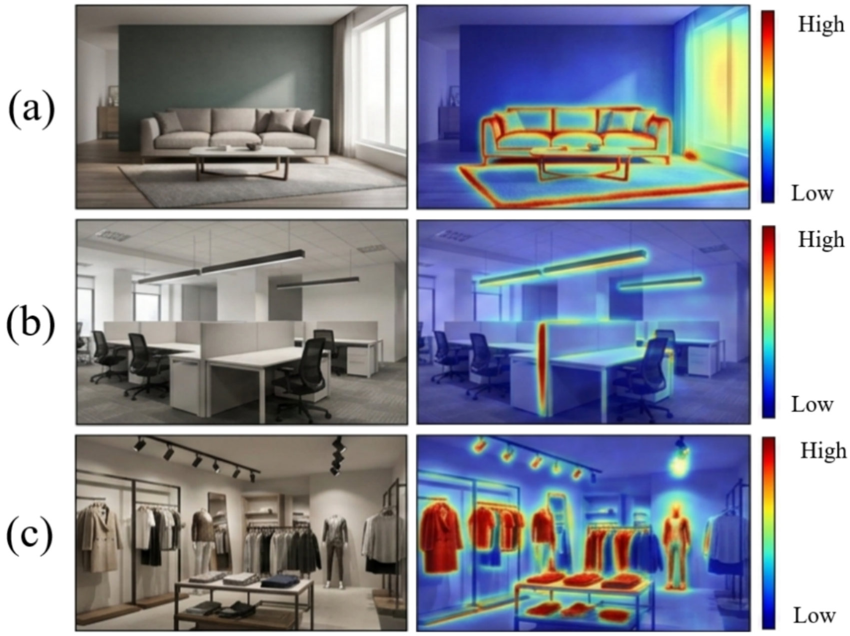

FIGURE 2. CNN Feature Activation Response: (a) Living room; (b) Office space; (c) Commercial exhibition space

area. Feature vectors encode the furniture arrangement and natural lighting distribution. The office scene corresponds to Figure 2(b), with activation peaks at the workstation partition edges and linear lighting fixtures. The desktop plane response level is moderate. Geometric regularity and artificial lighting layout information are incorporated into the extraction process. The commercial display scene is shown in Figure 2(c), with merchandise display shelves and mannequin positions highlighted by the heatmap. High-value clusters are generated by spotlight beams. The main extraction parameters for this space type consist of visual density and focal lighting. The mapping process from visual input to numerical descriptors does not rely on semantic labels; this is reflected by the activation patterns.

All elements of individual output vector are used as art dimension parameter in objective function. The process of visual feature extraction module and engineering performance simulation module is parallel. The feature vector data is sent to multi-objective optimization algorithm via interface. The model update process does not depend on human intervention. The digital twin adjusts its geometric topology and material parameters according to the feedback parameters.

AEM JOURNAL .ORG

C. PHYSICAL FIELD SIMULATION AND SURROGATE MODEL CONSTRUCTION FOR ENGINEERING PERFORMANCE

The airflow organization and structural stress state of the indoor thermal and humid environment are handled by CFD and FEA solvers. The governing equations of the fluid domain are described by the Navier-Stokes (N-S) equations for incompressible Newtonian fluids, which describe the mass and momentum conservation characteristics [29-30]. Transient flow behavior depends on the combined effects of the time term and the convection term; the diffusion term reflects the influence of viscous forces; the source term includes gravity and other volume force components.

$$\rho\left(\frac{\partial v}{\partial \tau}+v\cdot\nabla v\right)=-\nabla p+\mu\nabla^2 v+f_{\text{body}} \tag{7}$$

ρ represents air density; v represents the velocity vector; τ is the time variable; p refers to the pressure field; μ is the dynamic viscosity coefficient; f_{body} represents the force per unit volume. The structural domain is discretized into a finite element mesh; the nodal displacement field is solved through equilibrium equations; and the stress tensor is derived from the strain-displacement relationship and constitutive model. Thermal comfort PMV is calculated based on the human body thermal balance equation, and the difference between metabolic heat production and heat dissipation determines the value of the thermal sensation index.

$$\text{PMV}=[0.303\exp(-0.036M)+0.028]\cdot(\dot{Q}_{\text{gen}}-\dot{Q}_{\text{diss}}) \tag{8}$$

$\dot{Q}_{\text{gen}}$ is the internal heat production rate; $\dot{Q}_{\text{diss}}$ represents the heat dissipation rate to the environment; M represents the human metabolic rate. High-dimensional coupled simulation processes are accompanied by significant computational resource consumption, and directly calling the solver to support optimization iterations constrains efficiency. The RBF (Radial Basis Function) surrogate model establishes an approximate mapping relationship between design variables and engineering indicators, replacing high-precision physical field simulation [31-32]. The input vector consists of material reflectivity, spatial interface positioning, and pipeline path parameters, while the output vector corresponds to thermal comfort indicators and structural safety factors. Figure 3 presents the two-layer architecture of physical field simulation and surrogate model, demonstrating the parallel structure and data interaction interface between the high-precision solver and the fast prediction model.

In Figure 3, the high-fidelity physics solution layer receives the design variable vector. The samples, processed by LHS (Latin Hypercube Sampling), are then fed into the CFD solver and the FEA solver, respectively. The CFD solver outputs the thermal comfort PMV value based on the Navier-Stokes equations, while the FEA solver outputs the structural stress field based on the equilibrium equations. These two sets of data are combined to form the true value set of engineering indicators. The surrogate model fast prediction layer receives the true value set and performs sample data mapping. During model training, the RBF surrogate model parameters are determined by minimizing the mean square error. The design variable vector is directly input into the surrogate model to generate predicted values of engineering indicators. These predicted values are then fed back into a multi-objective optimization loop to correct the design variables. An offline training data generation link connects the high-fidelity physics solution layer and the surrogate model fast prediction layer, completing the migration of high-precision data to the fast prediction model.

Sample data is generated through LHS, achieving full coverage of the design space. The model training process minimizes the mean square error between the predicted values and the simulated true values to determine the weighting coefficients and center positions. The validation set data is used to evaluate the generalization ability of the surrogate model; the prediction accuracy must meet the input standards of the optimization algorithm. The updated proxy model incorporates a multi-objective optimization loop to enable real-time evaluation of engineering performance.

$$\hat{y}(d_1)=\sum_{j=1}^{N_{\text{rbf}}}\omega_j\phi(\|d_1-c_j\|) \tag{9}$$

$\hat{y}$ represents the predicted output of the surrogate model; d_1 represents the design variable vector; N_{rbf} is the number of basis function centers; ω_j represents the j-th weight coefficient; ϕ is the radial basis kernel function; c_j refers to the j-th center vector.

D. MULTI-OBJECTIVE OPTIMIZATION SOLUTION AND VIRTUAL VERIFICATION CLOSED LOOP

Based on NSGA-III, the multi-dimensional objective function vector integrates visual feature vectors, thermal comfort PMV, structural safety factor, and energy consumption per unit area to form the core evaluation cri teria for the optimization search. The optimization search space follows the dimensions of material reflectivity, spatial interface positioning coordinates, and pipeline path parameters determined in the aforementioned engineering performance simulation. The objective function mapping relationship is established through mathematical expressions, with each component corresponding to aesthetic quality, environmental comfort, structural stability, and energy efficiency indicators, respectively.

$$\text{Obj}(d)=[O_{\text{vis}}(d),O_{\text{pmv}}(d),O_{\text{str}}(d),O_{\text{eng}}(d)]^T \tag{10}$$

$\text{Obj}(d)$ is the multiobjective function vector, in which d is the design variable vector in the search space; O_{vis} is the aesthetic scoring function; O_{pmv} is the thermal comfort PMV function; O_{str} is the structural safety factor function; and O_{eng} is the energy consumption per unit area function.

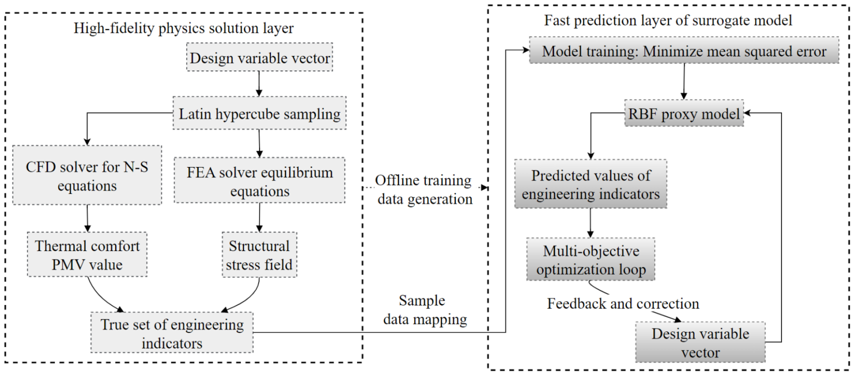

FIGURE 3. Two-layer architecture of physics simulation and surrogate model

The standard NSGA-III associates reference points using penalty-based boundary intersection distance, which suffers from association bias on non-convex Pareto fronts. The improved algorithm adopts perpendicular distance as the association metric, recalculates the extreme solution along each reference point direction in every generation, and applies a dynamic reference point scaling factor to eliminate dimensional differences among objectives. Continuous design variables are handled by simulated binary crossover and polynomial mutation with distribution indices set to 20 for both operators. Discrete design variables corresponding to material types and equipment selection undergo uniform crossover and bit-flip mutation with a crossover probability of 0.9 and a mutation probability of 0.1. In each generation, discrete and continuous variables are crossed and mutated separately before merging to form the offspring population. This mechanism ensures search efficiency and solution set uniformity in the high-dimensional mixed-variable space.

The improved NSGA-III maintains the population diversity with reference points; the association distance between individual and reference point is the selection pressure. In the process of population evolution, every individual is allocated to the nearest reference point direction, and then crowding degree is calculated by using vertical distance metric method. The association distribution between population individuals and reference points is shown in Figure 4.

Figure 4 shows the distribution of population individuals and reference points in the target space. Blue dots represent population individuals, and red asterisks mark the locations of reference points. Dashed lines connect individuals with their associated reference points, demonstrating the internal mechanism by which the algorithm maintains diversity and revealing the geometric relationship between the solution set distrib ution and the reference point orientation in the target space.

$$d_{\perp} = \frac{|(\mathrm{Obj}_{\mathrm{norm}} - Z_{\mathrm{ref}}) \cdot D_{\mathrm{dir}}|}{\|D_{\mathrm{dir}}\|} \tag{11}$$

$d_{\perp}$ is the perpendicular distance from the individual to the reference line; $\mathrm{Obj}_{\mathrm{norm}}$ is the normalized objective function vector; Z_{ref} is the coordinate vector of reference point in target space; D_{dir} is the direction vector of reference point; $\|\cdot\|$ is the vector norm operation. The population evolution process converges to the Pareto front. Then, the optimal variable parameters are fed back to update the digital twin model. Finally, the virtual mirror layer accepts the optimized geometric topology and material attribute data to update the BIM primitive state. The dynamic mapping function adjusts the attributes of virtual space according to the new variable value, and then updates the physical entity and virtual mirror synchronously.

$$S_{\mathrm{model}} = G(d^{*}, S_{\mathrm{curr}}) \tag{12}$$

S_{model} is the state matrix of digital twin model after update; G is the update mapping operator of model; d^{*} is the design variable vector in the Pareto optimal solution set; S_{curr} is the state matrix of current digital twin model. Closed-loop verification performs collision detection and performance recalculation within the virtual scenario to verify the feasibility of the optimization scheme. The corrected model data feeds back to update the digital twin model for subsequent design iterations. All optimization and verification activities remain confined to the design phase.

III. EXPERIMENTAL CASES AND PARAMETER CONFIGURATION

The experiment selects the publicly available 3D indoor space model dataset Structured3D as the geometric data support for the validation phase [33-34]. This dataset contains densely labeled information for over 3000 indoor spaces. The selection process narrows down the models to three functional types: living room, office space, and commercial display space, ultimately selecting a total of 500 models. Each model provides complete 3D geometric mesh data, and material annotation information and panoramic rendering views are included in the data package. The raw data undergoes format conversion and lightweight processing to reduce the number of model faces and enhance computational efficiency. Topological structure checks are performed to repair mesh defects, and texture coordinates are unified to eliminate texture misalignment. Coordinate systems and unit systems are unified to eliminate spatial position errors. The output of exchange files is adapted

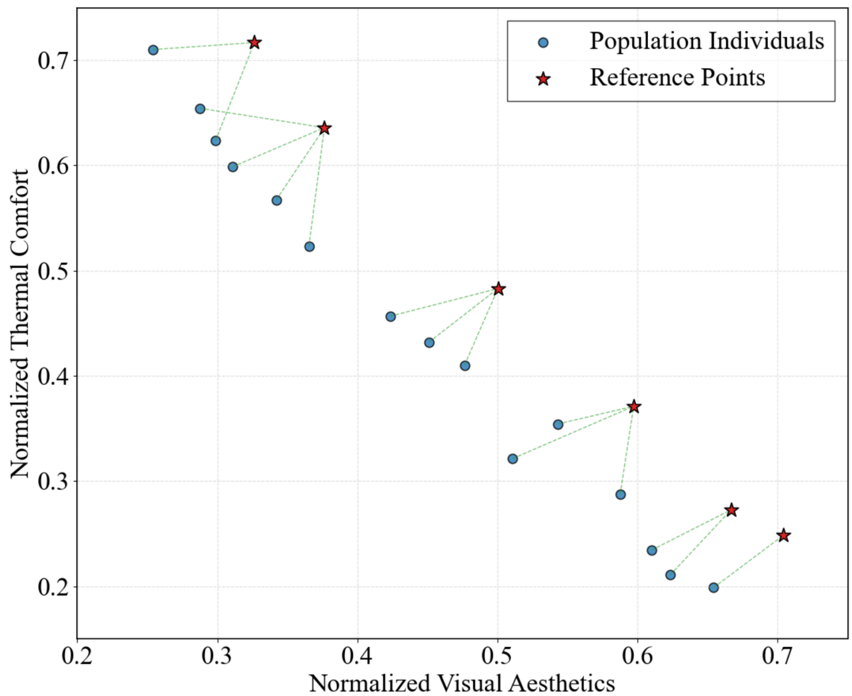

FIGURE 4. NSGA-III Reference Point Association Mechanism

to BIM software and simulation solvers to ensure lossless data transmission between different software platforms. The dataset is randomly divided into training, validation, and test sets in a 7:2:1 ratio, and the random partitioning strategy ensures that the sample distribution is statistically representative. The partitioned data is used for subsequent CNN training and evaluation, providing standardized input for the visual feature quantization module. This study employs a hardware platform with 2 Intel Xeon Gold 6330 CPUs and 128GB system memory to handle the large matrices. The graphics processor NVIDIA RTX A6000 is used to accelerate the CFD and FEA calculation and high-fidelity physics data processing. Autodesk Revit 2024 is employed for BIM management. ANSYS Fluent 2023 R2 and ANSYS Mechanical 2023 R2 are used as CFD and FEA software.

The PyTorch 2.0 framework is used to realize the CNN and NSGA-III algorithm. For the NSGA-III, the population size is set as 200 and the maximum number of generations as 500. The crossover probability is 0.9, and the mutation probability is 0.1. According to the target dimension, the number of reference points is set as 30. This configuration is used as a reference for the efficiency comparison in the following analysis.

The validity of method effectiveness is verified by the establishment of reference objects and the measure ment units. The evaluation framework is constructed with two representative methods as comparative baselines. The first type of reference objects is conventional parametric optimization methods based on design specifications. This method tunes design variables with static rule constraints. The building fire protection codes in the rule base and the space size limits are included. The method lacks a global search process. The second type of reference objects is a single-objective genetic algorithm only considering energy consumption and thermal comfort, because there is no global search process in this method.

Table 1 shows the configuration information of comparison method and evaluation indicator, including three data items: optimization strategy, objective dimension, and solution algorithm. The comparison item includes proposed method, method 1, and method 2. The proposed method uses multi-objective collaborative optimization strategy. Objective dimension includes four dimensions: aesthetics, thermal comfort, and structural energy consumption. Solution algorithm is NSGA-III. Method 1 uses static adjustment based on design specification constraints. Objective dimension is a binary value of specification compliance. Solution algorithm is an automatic verification rule using a verification mechanism. Method 2 uses single-objective genetic iterative optimization. Objective dimension is a two-dimensional index of energy consumption and thermal comfort. Solution algorithm is a standard genetic algorithm solver.

IV. RESULTS ANALYSIS

A. CONVERGENCE AND DISTRIBUTION CHARACTERISTICS ANALYSIS OF MULTI-OBJECTIVE OPTIMIZATION SOLUTION SETS

This study uses a digital twin technology and applies an improved NSGA-III to solve the conflicts among multiple objectives, such as aesthetic parameters, thermal comfort PMV, structural stress, and unit energy consumption. The base work verifies the evolutionary path of the solution set in objective space, and the reliability of global optimization process is validated. HV (Hypervolume) represents the

TABLE 1. Comparison of different optimization method configurations

Comparative item	Methods of this article	Baseline method 1	Baseline method 2
Optimization strategy	Multi-objective collaborative optimization strategy	Static adjustment constrained by design specifications	Single-objective genetic iterative optimization
Target dimension	Four dimensions of structural energy consumption for aesthetic thermal comfort	Specification Compliance Binary Determination	Energy consumption and thermal comfort dual-dimensional index
Solving algorithm	NSGA-III	Rule engine automatic verification mechanism	Standard genetic algorithm solver

volume of space dominated by the Pareto front and the reference point, and the numerical increase represents the enhance ment of convergence quality. SP (Spacing Metric) is the spacing metric, which can guarantee the diversity of multiple objective design scheme. The optimization process updates the computational model without any physical space modification during construction or operation phases. The iterative updating of digital twin model depends on above two metrics to adjust the exploration and utilization behaviors in searching process. The output performance of evolutionary generations can reflect the reliability of the optimization mechanism in complex coupling environment.

The dynamic change pattern of the metrics with the number of iterations are shown in Figure 5; the shaded area represents the standard deviation fluctuation range of multiple independent runs.

Figure 5(a) illustrates the evolution of convergence performance. The mean hypervolume increases from an initial 0.3142 to a final 0.8978, showing a significant increase in the early stage and then leveling off. The change in the curve slope reflects the algorithm's rapid location of the feasible region in the early stages, followed by a refined search. The standard deviation band gradually narrows with increasing generations, indicating reduced individual differences in the population and enhanced robustness. The elite preservation strategy ensures the transmission of high-quality genes, driving the continuous expansion of the dominant volume. Figure 5(b) illustrates the diversity distribution characteristics. The mean SP decreases from 0.6853 to 0.1241, with the decrease representing a more uniform distribution of the solution set. The rate of decrease slows down after 200 generations, indicating that the population diversity maintenance mechanism is effective. The width of the shaded area shrank synchronously, verifying the consistency of results from multiple runs. The reference point association mechanism in the high-dimensional target space prompts individuals to diffuse into unexplored areas, avoiding getting trapped in local optima. After receiving the optimization parameters, the digital twin model receives feedback from the physics simulation to further correct the solution set position. The data trend confirms that the improved NSGA-III performs stably in balancing convergence speed and distribution uniformity. The total optimization time for 500 generations is 124.5 seconds on the specified hardware platform, corresponding to 0.249 seconds per generation. The per-generation computational cost remains nearly constant because the RBF surrogate model replaces high-fidelity physical field simulations during evolutionary search.

B. COMPARISON OF AESTHETIC EFFECTS AND ENGINEERING PERFORMANCE BEFORE AND AFTER OPTIMIZATION

To solve the performance degradation problem induced by the splitting of aesthetic value and engineering logic in traditional interior design, this study chooses a typical office case and verifies the physical field distribution of the field before and after optimization using digital twin dynamic mapping mechanism. PMV is an important indicator to evaluate the human thermal comfort, coupling effect of airflow organization and temperature and humidity field; Von Mises stress reflects the equivalent stress state of components under the action of stress and represents the construction safety of components. The experiment chooses CFD and FEA solver to extract the typical physical quantity in the process of solving the physical quantity along the spatial profile and verify the performance difference of initial design and multi-objective collaborative optimization scheme. The improved NSGA-III-driven global optimization of design variables corrects the spatial interface and pipeline path parameters. The error bar represents the measurement uncertainty and numerical discretization error of IoT sensor; green shaded area represents the thermal comfort neutral range; the red warning line represents the material allowable stress limit. Figure 6 verifies the comparison of indoor thermal environment and structural performance profile before and after optimization and the change trend of physical field distribution.

Figure 6(a) shows the distribution of thermal comfort parameters along the profile. Generally, the initial design curve is above the comfort zone, and the maximum value is 1.56, which means that there is a large accumulation of heat in the local positions. After optimization, the curve is in the green shaded area; the value is between 0.31 and -0.12; the fluctuation range is significantly reduced. Airflow organization optimization changes the position of the air outlets and equipment layout. The abnormal temperature gradient points are removed, and the environmental uniformity is enhanced.

Figure 6(b) shows the distribution characteristics of structural stress field intensity. It can be seen that the initial design has exceeded the red warning line in several places, and the maximum value appearing in the mid-span area is 188.7 MPa. The optimized scheme changes the transmission path of force through topological structure adjustment, and the peak stress value is reduced to 142.3 MPa. The stress concentration around the column positions is alleviated. In addition, the data dispersion within the discretization error range has high data stability. Multi-physics coupled data

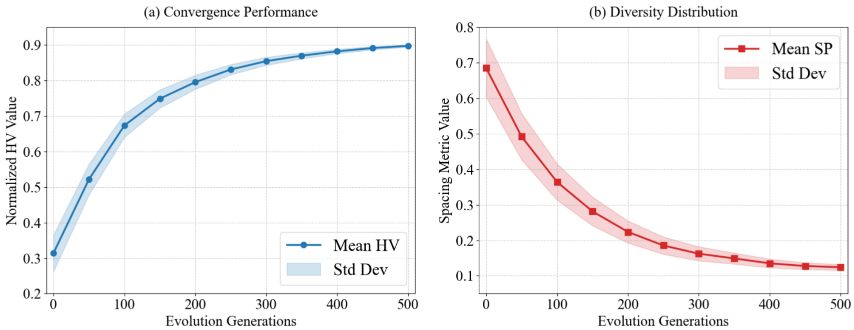

FIGURE 5. Convergence and Diversity Performance Indicators of the NSGA-III Algorithm: (a) Convergence Performance; (b) Diversity Distribution

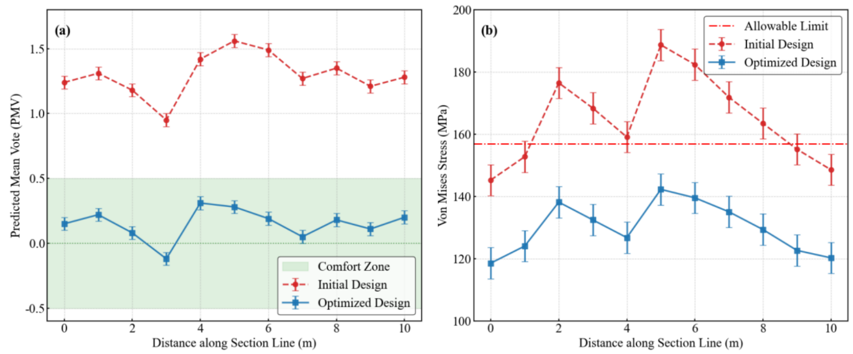

FIGURE 6. Comparison of indoor thermal environment and structural performance profiles before and after optimization: (a) Profile distribution of indoor thermal comfort PMV values; (b) Profile distribution of structural Von Mises stress

drives the correction of design variables, and then meets the visual aesthetics constraints and physical performance constraints. The digital twin model enables the iterative development of artistic form and engineering indicators in a synchronized way, solves the structural conflict, and verifies the effectiveness of the method in actual physical scenario.

C. PERFORMANCE COMPARISON OF VARIOUS OPTIMIZATION METHODS

To evaluate the actual effectiveness of the actual effectiveness of the multi-objective collaborative optimization framework applied in interior design field, this study randomly chooses three different strategies for horizontal comparison. The method proposed in this paper is based on digital twins and improved NSGA-III to solve for four dimension objectives simultaneously, namely aesthetics, thermal, structure safety, and energy consumption, so as to couple artistic and engineering parameters.

Baseline method 1 is based on static adjustment with respect to hard constraints of design specification and an automatic verification mechanism from rule engine; it is merely used for passive specification compliance evaluation with only binary evaluation ability but not global search ability.

Baseline method 2 is based on single-objective genetic iterative optimization, which only optimizes two dimensions of energy consumption and thermal comfort without considering artistic dimension and structural constraint.

The evaluation system consists of the following indicators: time consumed in a single optimization to evaluate computational efficiency, HV to evaluate the quality and dispersion of Pareto solution set, aesthetic scoring to evaluate the magnitude of visual feature vector, and the compliance rate of different engineering aspects to evaluate the physical field statistical compliance rate of different engineering aspects. All these indicators together form the multidimensional evaluation matrix. The specific numerical distribution is shown in Table 2.

In Table 2, the single-run optimization time of the proposed method remains at 124.5 seconds, lower than the baseline method 2's 185.3 seconds. This is because the RBF surrogate model replaces the high-precision physical field simulation process, reducing computational load while maintaining prediction accuracy. The HV reaches 0.8978, higher than the baseline method 2's 0.4520, reflecting the expansion of the solution set dominance volume and improved convergence accuracy in the four-dimensional target space, proving the effectiveness of the multi-objective search strategy. The aesthetic score of 8.74 points exceeds the baseline methods' scores of 5.12 and 5.35 points respectively, validating the role of CNN feature extraction in improving design quality and filling the gap in artistic quantification. The thermal comfort compliance rate of 96.4% and the structural safety compliance rate of 98.2% remain high. Although the baseline method 1 achieves a structural compliance rate of 95.0%, its unit energy consumption compliance rate is only 79.3%, reflecting the lack of a performance proactive optimization mechanism in static rules, leading to

TABLE 2. Comparison of performance indicators of different optimization methods

Metric	Proposed method	Baseline 1 method	Baseline 2 method
Time taken per optimization (s)	124.5 ± 10.2	38.6 ± 5.4	185.3 ± 15.6
HV index	0.8978 ± 0.032	-	0.4520 ± 0.045
Aesthetic rating (0-10)	8.74 ± 0.42	5.12 ± 1.15	5.35 ± 0.98
Thermal comfort compliance rate	96.4%	82.5%	91.7%
Structural safety compliance rate	98.2%	95.0%	88.4%
Unit energy consumption compliance rate	95.8%	79.3%	92.1%

energy efficiency losses. The structural safety compliance rate of the baseline method 2 drops to 88.4%, attributed to the single-objective solver ignoring structural constraints, posing a safety risk. The synergistic improvement of multi-dimensional indicators confirms that the global optimization mechanism driven by digital twins effectively balances the conflict between aesthetic value and engineering technology, achieving the goal of high-performance construction.

Additional comparison experiments are conducted between the improved NSGA-III and three baseline multiobjective algorithms under identical experimental conditions. Table 3 reports the mean hypervolume after 500 generations and the total optimization time for each algorithm.

TABLE 3. Performance comparison between improved NSGA-III and baseline multi-objective algorithms

Algorithm	Mean hypervolume (500 generations)	Total optimization time (s)
Improved NSGA-III	0.8978	124.5
Standard NSGA-III	0.7543	243.6
NSGA-II	0.7120	258.3
MOEA/D	0.7381	235.7

Notes: All algorithms use the same population size of 200, maximum generations of 500, crossover probability of 0.9, and mutation probability of 0.1. Standard NSGA-III employs penalty-based boundary intersection distance for reference point association. NSGA-II uses crowding distance sorting. MOEA/D uses Tchebycheff decomposition. The proposed method incorporates perpendicular distance association.

The comparison in Table 3 further demonstrates that the proposed modifications yield higher hypervolume and lower computational cost than standard NSGA-III, NSGA-II, and MOEA/D.

D. SENSITIVITY IDENTIFICATION OF KEY DESIGN VARIABLES

To explain the specific reasons for the performance fluctuations, it is important to understand the quantitative mapping relationship of objective function with design parameters. Material reflectivity has a great influence on the view and light distribution characteristic; spatial segmentation and positioning coordinates define airflow organization path and load transfer rule; integrated pipeline elevation affects equipment routing path and structural interference risk; evaluation system considers aesthetic quality from visual feature vector, thermal comfort from PMV, structure safety factor from stress level, and unit area energy consumption from performance indicator; normalized sensitivity coefficient reflects the marginal performance change caused by small variation of variable; two variables are compared in a high-dimension space after eliminating dimensionality with normalized marginal change rate of integrated sensitivity function; digital twin model captures high-dimension coupling relationship between input variable and output indicator through surrogate model; improvement NSGA-III iterative process records variation path of variables; structural safety indicator is calculated and normalized based on Von Mises stress field.

Table 4 presents the numerical results of the calculated sensitivity of key design variables under the given objective function. The data reflects the comprehensive contribution of variables to system performance, showcasing the quantitative reference dimensions for design decisions.

In Table 4, the sensitivity coefficients of the pipeline's overall elevation in terms of unit energy consumption and structural safety reach 0.895 and 0.882, respectively. This is because changes in elevation directly alter the duct resistance path and the probability of beam-column collisions, and fluid resistance and structural interference respond dramatically to changes in geometric position. Spatial separation and positioning coordinates have a weight of 0.781 on thermal comfort PMV. Geometric layout adjustments reconstruct the indoor airflow organization, and changes in boundary conditions lead to significant fluctuations in thermal environment parameters. Material reflectivity contributes 0.824 to aesthetic quality but only shows a weak correlation of 0.041 in structural safety indicators. Surface optical properties do not participate in the mechanical transmission process, and the visual feature extraction mechanism is independent of physical field simulation. Engineering variables dominate physical performance, while artistic parameters mainly drive visual evaluation results, indicating a clear functional decoupling between variables. The sensitivity differences among multidimensional objectives reveal the distribution pattern of coupling strength between design variables and performance indicators. Key variable identification provides a priority basis for subsequent differentiated spatial optimization and supports the dynamic update strategy of the digital twin.

TABLE 4. Normalized sensitivity coefficients of key design variables with respect to the multidimensional objective function

Design variables	Aesthetic quality	Thermal Comfort PMV	Structural safety	Unit energy consumption	Overall sensitivity
Material reflectivity	0.824	0.153	0.041	0.387	0.351
Spatial Separation Positioning Coordinates	0.452	0.781	0.695	0.314	0.561
Pipeline integrated elevation	0.128	0.546	0.882	0.895	0.613

E. COMPARISON OF SPATIAL OPTIMIZATION RESULTS FOR DIFFERENT FUNCTIONAL TYPES

Living room space satisfies the function of daily living, and design quality requires visual harmony and satisfaction. Office space satisfies the function of work, which has strict requirements for thermal uniformity and structure reliability. Commercial display space satisfies the function of image display to attract customers, and large amounts of lighting and display devices increase the energy consumption. Is aesthetic score, the larger the magnitude of the vector extracted by visual features from CNN, PMV is used to quantify thermal comfort; structural safety factor is defined as the ratio of allowable material stress and actually calculated material stress; energy consumption per unit area reflects the economic type of space operation, and these four types of indicators together constitute the evaluation indicators of multi-objective optimization solution. Pareto optimal solution sets for the three functional types—living room, office space, and commercial display space—are aggregated, and box plots are drawn to reveal the distribution characteristics under each objective dimension. In Figure 7, the red line segment marks the median position, with the upper and lower boundaries of the box corresponding to the third and first quartiles, respectively. The beard extends to the minimum and maximum values, visually presenting the central tendency and dispersion of the solution set.

In the distribution of aesthetic scores of Figure 7(a), the median value of aesthetic scores of commercial display spaces is 9.1, higher than that of office spaces (8.2), which means commercial spaces pursue more visual effects. Office spaces have smaller cabinet spans, which means a high degree of design standardization and no fluctuation; while commercial spaces get the highest score, but their cabinet spans are slightly larger. Pursuing high aesthetic scores is still possible with some diversity in design in commercial spaces due to the same reasoning that they have the highest requirement in exhibition style. Commercial spaces rely on effects and focal lights to attract customers, so designers tend to provide higher aesthetic scores while office spaces are restricted by the principle of prioritizing function, which limits the lower and upper limits of aesthetic scores. The thermal comfort PMV analysis of Figure 7(b) shows office buildings near the feeling of being in the middle of the neutral temperature, median value of 0.05 and cabinets narrower cabinets reflect the strict control over the human comfort; commercial cabinets median 0.3, the maximum value of up to 0.8, due to the disturbance of the local thermal environment caused by the continuous heating of high-power lighting equipment, indicating some degree of comfort at the expense of display effects in the design.

Figure 7(c) shows that the structural safety factor is highest in office spaces, with a median of 1.8 and an overall upward shift in distribution, reflecting the redundancy requirement for structural reserves. Commercial exhibition spaces, due to frequent changes in exhibition layout leading to load uncertainty, have a median of 1.5 and a minimum lower bound of 1.2, indicating a design focus on flexibility rather than high-strength reserves.

Figure 7(d) shows the most significant differences in unit energy consumption. The median energy consumption in commercial spaces (85 kWh/m^2·a) is much higher than that in living rooms (45 kWh/m^2·a), extending to 105 kWh/m^2·a, reflecting the inevitable energy cost of high-i ntensity lighting and equipment heat dissipation. The low energy consumption dispersion in living rooms stems from the relatively stable living behavior patterns. The differentiated distribution of the three types of spaces across the four objectives demonstrates that functional needs dominate the trade-off between art and engineering indicators, and the multi-objective optimization framework effectively captures and presents this inherent law.

F. VALIDATION OF AESTHETIC SCORING AGAINST HUMAN JUDGMENT

To validate the aesthetic scores output by the convolutional neural network, a human evaluation study is conducted. One hundred interior scene renderings are randomly selected from the test set held out during CNN training. Ten interior designers with at least five years of professional experience independently rate each image on a zero to ten scale. The Pearson correlation coefficient between the CNN predicted scores and the mean human ratings is 0.892, indicating a strong positive linear relationship. The intraclass correlation coefficient among the ten expert ratings is 0.914, demonstrating high inter-rater reliability. The mean absolute error between the CNN scores and individual expert ratings is 0.68. These statistical results confirm that the CNN produces aesthetic assessments closely aligned with human expert judgment.

TABLE 5. Validation of CNN aesthetic scores against human expert ratings

Metric	Value	Interpretation
Pearson correlation coefficient	0.892	Strong positive correlation
Intraclass correlation coefficient	0.914	High inter-rater reliability
Mean absolute error	0.68	Low absolute deviation

V. CONCLUSION

This paper constructs a digital twin-driven collaborative optimization framework to address the disconnect between

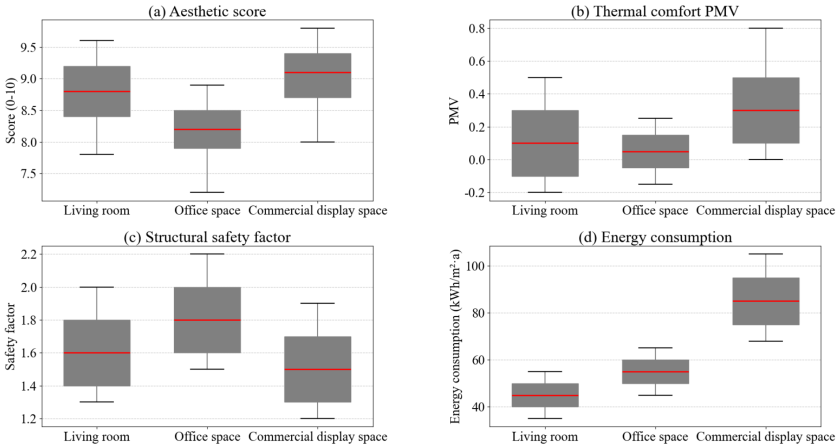

FIGURE 7. Comparison of multi-objective optimization results for different functional types of space: (a) Aesthetic score; (b) Thermal comfort PMV; (c) Structural safety factor; (d) Energy consumption

aesthetic value and engineering logic in interior design. By integrating real-time IoT data and BIM, a dynamic twin achieves high-fidelity mapping between physical entities and virtual mirrors. CNN extracts visual feature vectors to quantify aesthetic indicators, and CFD and FEA are combined to solve for thermal comfort and structural stress fields, forming a multi-dimensional objective function. An improved NSGA-III-driven global optimization obtains a Pareto optimal solution set for both artistic effect and engineering indicators. Multi-physics coupled data drives design variable correction, balancing visual aesthetics and physical constraints.

Aesthetic score, thermal environment uniformity, and structural safety are enhanced, while energy consumption per unit area is controlled in experimental results. The optimization results of spaces with different uses show a differentiated distribution, which further verifies the correctness and effectiveness of the framework in dealing with complex scenarios. This study establishes a deep coupling relationship between aesthetic value and engineering, and explores a technical route to optimize the whole lifecycle cost of interior space and to drive the digitalization of the construction industry.

AUTHOR CONTRIBUTIONS

Jingjing Tao contributed to this article as a sole author and have read and agreed to the published version of the manuscript.

CONFLICTS OF INTEREST

The author declares no conflict of interest.

FUNDING

This research received no external funding.

ACKNOWLEDGEMENTS

Not applicable.

REFERENCES

[1] S. Banihashemi, A. Assadimoghadam, A. Hajirasouli, K. LeNguyen, and S. R. Mohandes, "Parametric design in construction: a new paradigm for quality management and defect reduction," International Journal of Construction Management, vol. 25, no. 13, pp. 1534-1551, 2025, doi: 10.1080/15623599.2024.2447653.

[2] W. A. Muhsin , "Contemporary Design Strategies and their Role in Enhancing the Functional and Aesthetic Values of Industrial Product," Online Journal of Art & Design, vol. 12, no. 4, pp. 22-37, 2024, doi: https://www.adjournal.net/ articles/124/1243.pdf.

[3] J.F. Yao, Y. Yang, X.C. Wang , and X.P. Zhang, "Systematic review of digital twin technology and applications," Visual computing for industry, biomedicine, and art, vol. 6, no. 1, pp. 10-29, 2023, doi: 10.1186/s42492-023-00137-4.

[4] Y. Wang, X. Wang, A. Liu, J. Zhang, and J. Zhang, "Ontology of 3D virtual modeling in digital twin: a review, analysis and thinking," Journal of Intelligent Manufacturing, vol. 36, no. 1, pp. 95-145, 2025, doi: 10.1007/s10845-023-02246-6.

[5] O. Pylypchuk, "Coloristic levels of perception of an art object in the interior space," Cultura e Scienza del Colore-Color Culture and Science, vol. 16, no. 2, pp. 100-107, 2024, doi: 10.23738/CCSJ.160210.

[6] M. Khanzadeh, "Beyond Aesthetics: Emotion, Atmosphere, and Cultural References through Color in Interior Architecture," Journal of Academic Social Science Studies, vol. 17, no. 101, pp. 49-63, 2024, doi: 10.29228/JASSS.77266.

[7] H. Wang, "An investigation into the evaluation and optimisation method of environmental art design based on image processing and computer vision," Scalable Computing: Practice and Experience, vol. 26, no. 1, pp. 277-286, 2025, doi: 10.12694/scpe.v26i1.3518.

[8] F. Deng, S. Wei, Y. Xu, and H. Li, "Damage identification of long-span bridges based on the correlation of monitored global dynamic responses in high dimensional space," Engineering Structures, vol. 299, no. 1, pp. 117134-117144, 2024, doi: 10.1016/j.engstruct.2023.117134.

[9] H. Jain, "Critical insights into thermal comfort optimization and heat resilience in indoor spaces," City and Built Environment, vol. 2, no. 1, pp. 14-39, 2024, doi: 10.1007/s44213-024-00038-z.

[10] G.A. Ascanio, "Building intelligence at the interior scale: Systems integration in high-end residential design," IPHO-Journal of Advance Research in Science And Engineering, vol. 3, no. 12, pp. 52-60, 2025, doi: https://doi.org/10.5281/ zenodo.19355214.

[11] M. Jiang, X. Rui, F. Yang, W. Zhu, H. Zhu, and W. Han, "Design and dynamic performance research of MR hydro-pneumatic spring based on multi-physics coupling model," Nonlinear dynamics, vol. 111, no. 9, pp. 8191-8215, 2023, doi: 10.1007/s11071-023-08279-z.

[12] Y. Li, Q. Zhao, M. Yang, Z. Ma, and X. Hei, "Advancements and Applications of Industry Foundation Classes Standards in Engineering: A Comprehensive Review," Buildings, vol. 15, no. 16, pp. 2927-2957, 2025, doi: 10.3390/buildings15162927.

[13] B. Liu, "The analysis of art design under improved convolutional neural network based on the Internet of Things technology," Scientific Reports, vol. 14, no. 1, pp. 21113-21131, 2024, doi: 10.1038/s41598-024-72343-w.

[14] M. Vijendran, J. Deng, S. Chen, S. Ho E, and P. Shum H, "Artificial intelligence for geometry-based feature extraction, analysis and synthesis in artistic images: a survey," Artificial Intelligence Review, vol. 58, no. 2, pp. 64-110, 2024, doi: 10.1007/s10462-024-11051-3.

[15] W. Li, "Enhanced automated art curation using supervised modified CNN for art style classification," Scientific Reports, vol. 15, no. 1, pp. 7319-7335, 2025, doi: 10.1038/s41598-025-91671-z.

[16] Y. Lin, B. Wang, and Z. Fan, "CNN-driven art design decision support system based on big data," Computer-Aided Design & Applications, vol. 21, no. S21, pp. 37-52, 2024, doi: 10.14733/cadaps.2024.S21.37-52.

[17] A. Cernei, F. Thevenet, F. Bode, M. Verriele, and I. Nastase, "Critical Review of Current Validation Methodologies and Future Developments in CFD-Based Indoor Environmental Quality Analysis," Indoor Air, vol. 2025, no. 1, pp. 6601284-6601328, 2025, doi: 10.1155/ina/6601284.

[18] D. Isobe and Q. Yang, "An integrated finite element analysis and virtual reality system for structural and indoor nonstructural components of buildings under seismic excitations," Journal of Building Engineering, vol. 98, no. 1, pp. 111320-111346, 2024, doi: 10.1016/j.jobe.2024.111320.

[19] H. Li, Y. Yuan, D. Wu, Y. Fan, and F. Jiang, "Optimizing of architectural geometry and tubular daylight guidance system based on genetic algorithm to enhance daylighting and energy performance in underground office buildings," Journal of Building Engineering, vol. 86, no. 1, pp. 108895-108915, 2024, doi: 10.1016/j.jobe.2024.108895.

[20] J. Ratajczak, D. Siegele, and E. Niederwieser, "Maximizing energy efficiency and daylight performance in office buildings in BIM through RBFOpt model-based optimization: The GENIUS project," Buildings, vol. 13, no. 7, pp. 1790-1809, 2023, doi: 10.3390/buildings13071790.

[21] X. Li, X. Li, G. Hu, Q. Niu, and L. Xu, "A low-cost 3D mapping system for indoor scenes based on 2D LiDAR and monocular cameras," Remote Sensing, vol. 16, no. 24, pp. 4712-4735, 2024, doi: 10.3390/rs16244712.

[22] X. Lin, B. Xue, and X. Wang, "Digital 3D reconstruction of ancient Chinese great wild goose pagoda by TLS point cloud hierarchical registration," ACM Journal on Computing and Cultural Heritage, vol. 17, no. 2, pp. 1-16, 2024, doi: 10.1145/3639932.

[23] A. Tenorio-Trigoso, M. Castillo-Cara, G. Mondragon-Ruiz, C. Carrion, and B. Caminero, "An analysis of computational resources of event-driven streaming data flow for internet of things: A case study," The Computer Journal, vol. 66, no. 1, pp. 47-60, 2023, doi: 10.1093/comjnl/bxab143.

[24] D. Shvaika, A. Shvaika, and V. Artemchuk, "MQTT broker architectural enhancements for high-performance P2P messaging: TBMQ scalability and reliability in distributed IoT systems," IoT, vol. 6, no. 3, pp. 34-57, 2025, doi: 10.3390/iot6030034.

[25] D. Zhu, G. Jiang, X. Liu, X. Zhao, Y. Shen, and J. Luo, "Digital twin-enabled subgrade monitoring: a BIM-integrated data management and visualization," Engineering Research Express, vol. 7, no. 2, pp. 025129-025145, 2025, doi: 10.1088/2631-8695/ade1a5.

[26] C. Biagini, A. Bongini, and L. Marzi, "From BIM to digital twin," IOT data integration in asset management platform. Journal of Information Technology in Construction, vol. 29, no. 1, pp. 1103-1127, 2024, doi: 10.36680/j.itcon.2024.049.

[27] M. Guo, X. Wu, H. Qi, Y. Zhang, J. Chen, Y. Wei, X. Shang, et al., "A methodology for sky-space-ground integrated remote sensing monitoring: A digital twin framework for multi-source Data-BIM integration in residential quality monitoring," Journal of Building Engineering, vol. 102, no. 1, pp. 111976-111996, 2025, doi: 10.1016/j.jobe.2025.111976.

[28] N. Albelwi, "DT-LCAF: Digital Twin-Enabled Life Cycle Assessment Framework for Real-Time Embodied Carbon Optimization in Smart Building Construction," Sustainability, vol. 18, no. 5, pp. 2321-2345, 2026, doi: 10.3390/su18052321.

[29] J.R. Shin, "General solutions to the Navier-Stokes equations for incompressible flow," Journal of Ocean Engineering and Technology, vol. 38, no. 5, pp. 315-324, 2024, doi: 10.26748/KSOE.2024.051.

[30] H. Youssef, A. Elmelouky, M. Louzazni, F. Belhora, and M. Monkade, "A numerical study of interface dynamics in fluid materials," Materiaux & Techniques, vol. 112, no. 4, pp. 401-421, 2024, doi: 10.1051/mattech/2024018.

[31] A. Hashemi, J. Jang, and J. Beheshti, "A machine learning-based surrogate finite element model for estimating dynamic response of mechanical systems," IEEE Access, vol. 11, no. 1, pp. 54509-54525, 2023, doi: 10.1109/ACCESS.2023.3282453.

[32] G. Tomassetti, "Direct and surrogate optimization in applied superconductivity: state of the art, perspectives and challenges," Superconductor Science and Technology, vol. 38, no. 7, pp. 073001-073021, 2025, doi: 10.1088/1361-6668/adea1b.

[33] M. Brunklaus, M. Kellner, and A. Reiterer, "Three-Dimensional Instance Segmentation of Rooms in Indoor Building Point Clouds Using Mask3D," Remote Sensing, vol. 17, no. 7, pp. 1124-1150, 2025, doi: 10.3390/rs17071124.

[34] G. Pintore, F. Bettio, M. Agus, and E. Gobbetti, "Deep scene synthesis of Atlanta-world interiors from a single omnidirectional image," IEEE Transactions on Visualization and Computer Graphics, vol. 29, no. 11, pp. 4708-4718, 2023, doi: 10.1109/TVCG.2023.3320219.